$Na_2Y_3Cl_3[TeO_3]_4$: Synthesis, Crystal Structure and Spectroscopic Properties of the Bulk Material and its Luminescent Eu^{3+}-doped Samples

Sabine Zitzer, Frank Schleifenbaum and Thomas Schleid

University of Stuttgart, Institute for Inorganic Chemistry, Pfaffenwaldring 55, D-70569 Stuttgart, Germany

Reprint requests to Prof. Dr. Thomas Schleid. Fax: +49(0)711/685-64241.
E-mail: schleid@iac.uni-stuttgart.de

Z. Naturforsch. **2014**, *69b*, 150 – 158 / DOI: 10.5560/ZNB.2014-3274
Received September 30, 2013

Colorless, platelet-shaped single crystals of $Na_2Y_3Cl_3[TeO_3]_4$ were synthesized by a reaction of Y_2O_3 and TeO_2 (molar ratio 3 : 8) in evacuated silica ampoules within five days at 775 °C with an excess of NaCl added as flux and reagent. The new quintenary compound crystallizes in the monoclinic space group $C2/c$ with the lattice parameters $a = 2380.69(14)$, $b = 552.76(3)$, $c = 1662.48(9)$ pm, $\beta = 134.045(3)°$ and $Z = 4$. The crystal structure presents one of the rare oxotellurates(IV) containing isolated $[TeO_3]^{2-}$ units, which could be verified by Raman spectroscopy. Doping with Eu^{3+} (3 mass-%) at the Y^{3+} sites in eightfold oxygen coordination leads to a strong orange-red luminescence of $Na_2Y_3Cl_3[TeO_3]_4$:Eu^{3+} under UV excitation with a wavelength of $\lambda = 254$ nm. Beyond the electronic Eu^{3+} transitions of the $4f^6$ state, the fluorescence excitation spectrum shows an intense broad charge-transfer band resulting from both $O^{2-} \rightarrow Eu^{3+}$ ligand-to-metal charge-transfer (LMCT) as well as electronic Eu^{3+} $d \rightarrow f$ and Te^{4+} $s \rightarrow p$ transitions. The emission spectrum features the prominent $f \rightarrow f$ transitions of Eu^{3+}-doped oxidic compounds. The optical band gaps of the undoped and doped samples were determined by diffuse reflectance spectroscopy revealing just minimal doping effects on the crystal structure. The optical band gaps could be assigned in the excitation spectrum in the charge-transfer broad-band region supporting the assumption of an inorganic antenna effect of the Te^{4+} cations.

Key words: Yttrium, Oxotellurates(IV), Crystal Structures, Spectroscopy, Eu^{3+} Luminescence

Introduction

There are only few compounds among the rare-earth metal(III) oxotellurates(IV) exhibiting crystal structures with isolated $[TeO_3]^{2-}$ units, meaning that these complex anionic entities are present without any secondary interactions between one another. All ternary compounds with the compositions $M_2Te_3O_9$ [1 – 6], $M_2Te_4O_{11}$ [7 – 13], and $M_2Te_5O_{13}$ [14 – 18] (M = Sc, Y, La; Ce–Lu) show strong interactions among their $[TeO_3]^{2-}$ groups. With the incorporation of halide anions into these compounds (*e. g.* $Y_{11}ClTe_{16}O_{48}$ [19, 20], $Y_6Br_4Te_{11}O_{29}$ [21] or $HoClTe_2O_5$ [22]), the space between the $[TeO_3]^{2-}$ units is expanded, so that in the crystal structures both isolated and condensed $[TeO_3]^{2-}$ anions can be found. The complete absence of those interactions was not only realized for $HoCl[TeO_3]$ [23], but also in the cationic and anionic derivatives $Na_2M_3X_3[TeO_3]_4$ with X = Br and I [24, 25], which structurally resemble very much the title compound $Na_2Y_3Cl_3[TeO_3]_4$. Especially yttrium compounds are usually employed for the preparation of potential host structures for luminescent materials, since the lack of excitable $4f$ states implies no energy loss by internal conversion. Selected examples are the red light emitting phosphors Y_2O_2S:Eu^{3+} [26] and $Y[VO_4]$:Eu^{3+} [27], or in particular the yttrium(III) oxotellurates(IV) $Y_2Te_4O_{11}$:Eu^{3+} and $Y_2Te_5O_{13}$:Eu^{3+} [28]. The latter three show their Y^{3+} cations solely in low-symmetry first coordination spheres of mostly eight hard O^{2-} anions, just like in the case of $Na_2Y_3Cl_3[TeO_3]_4$:Eu^{3+}.

Experimental Section

Syntheses of $Na_2Y_3Cl_3[TeO_3]_4$ and its Eu^{3+}-doped samples

As starting materials Y_2O_3 (99.9%; ChemPur, Karlsruhe, Germany), TeO_2 (99.9995%, Alfa Aesar, Karlsruhe, Germany), NaCl (99.9%, Merck, Darmstadt, Germany), YCl_3 (99.9%; ChemPur, Karlsruhe, Germany), and Eu_2O_3 (99.9%, ChemPur, Karlsruhe, Germany) were used as received commercially. Colorless single crystals of the new compound $Na_2Y_3Cl_3[TeO_3]_4$ were obtained by a solid-state reaction of Y_2O_3 and TeO_2 weighed under argon atmosphere into silica ampoules in a 3 : 8 molar ratio with an excess of NaCl as flux and reactant. The evacuated and torch-sealed ampoules were heated at 775 °C for five days in a muffle furnace and subsequently cooled to room temperature within 50 h. First a reaction according to Eq. 1 took place,

$$3\,Y_2O_3 + 8\,TeO_2 + 6\,NaCl \rightarrow 2\,Na_2Y_3Cl_3[TeO_3]_4 + Na_2O \quad (1)$$

later followed under optimized synthetic conditions by the process shown in Eq. 2.

$$4\,Y_2O_3 + 12\,TeO_2 + YCl_3 + 6\,NaCl \rightarrow 3\,Na_2Y_3Cl_3[TeO_3]_4 \quad (2)$$

The raw products were washed with demineralized water to remove the excess of the fluxing chlorides (NaCl and YCl_3). The products showed colorless platelet-shaped single crystals, suitable for single-crystal X-ray diffraction studies. The europium-doped compound $Na_2Y_3Cl_3[TeO_3]_4$:Eu^{3+} was synthesized analogously to the solid-state reaction (Eq. 2) described above, which was performed with 3 mass-% of Eu_2O_3 as an additional component instead the corresponding part of pure Y_2O_3. In order to determine the purity of the products, powder X-ray diffraction measurements were carried out, showing phase-pure compounds on the level of X-ray diffraction (XRD, Fig. 1). The presumed by-product Na_2O from Eq. 1 could not be detected in the powder diffractogram, since it has been taken up by the inner wall of the silica ampoules in an acid-base reaction with SiO_2, most probably forming glassy Na_2SiO_3 or $Na_4[SiO_4]$.

X-Ray diffractometry and structure determination

The powder X-ray diffractograms were recorded with a STADI P diffractometer (Stoe, Darmstadt, Germany) using a position-sensitive detector and germanium-monochromatized CuK_α radiation (λ = 154.06 pm). The angular range was adjusted to $7° \leq 2\theta \leq 75°$ with a step width of 0.1° at room temperature. A comparison of the experimental powder diffractogram to the pattern simulated from single-crystal data confirmed a phase-pure product $Na_2Y_3Cl_3[TeO_3]_4$ (Fig. 1).

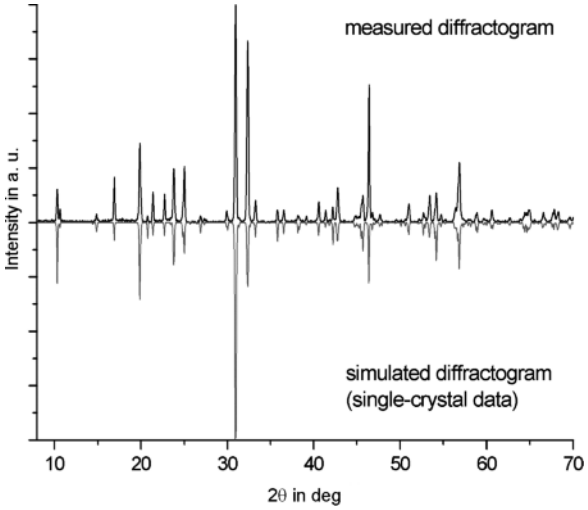

Fig. 1. Measured powder X-ray diffractogram of $Na_2Y_3Cl_3[TeO_3]_4$ in comparison with the simulated one from single-crystal data.

An intensity data set for a colorless, transparent and platelet-shaped single crystal of $Na_2Y_3Cl_3[TeO_3]_4$ was collected at room temperature on a κ-CCD X-ray diffractometer (Bruker-Nonius, Karlsruhe, Germany). The device uses graphite-monochromatized MoK_α radiation (λ = 71.07 pm). A numerical absorption correction was performed on the basis of the program HABITUS [29]. The structure solution and refinement was accomplished using the program package SHELXS/L-97 [30 – 32]. Details of the data collection and the structure refinement are summarized in Table 1. Atomic positions and coefficients of the equivalent isotropic displacement parameters are presented in Table 2. The motifs of mutual adjunction [33 – 35] can be taken from Table 3. Selected interatomic distances and bond angles are shown in Table 4.

Further details of the crystal structure investigation of $Na_2Y_3Cl_3[TeO_3]_4$ may be obtained from Fachinformationszentrum Karlsruhe, 76344 Eggenstein-Leopoldshafen, Germany (fax: +49-7247-808-666; e-mail: crysdata@fiz-karlsruhe.de, http://www.fiz-karlsruhe.de/request_for_deposited_data.html) on quoting the deposition number CSD-426510.

Raman spectroscopy

The Raman-spectroscopic data were measured at room temperature on a RFS/100S spectrometer (Bruker Optics, Ettlingen, Germany) in the spectral range of 150 – 3500 cm^{-1} and with a resolution of 4 cm^{-1} (Nd-YAG laser, λ = 1064 nm). The spectrum shows the four antici-

Table 1. Crystallographic data and numbers pertinent to data collection and structure refinement of $Na_2Y_3Cl_3[TeO_3]_4$.

Crystal system		monoclinic
Space group		$C2/c$ (no. 15)
Formula units		4
Lattice parameters	a, pm	2380.69(14)
	b, pm	552.76(3)
	c, pm	1662.48(9)
	β, deg	134.045(3)
Calculated density	D_x, g cm^{-3}	4.74
Molar volume	V_m, cm^3 mol^{-1}	236.75(2)
$F(000)$, e		1976
Index range	$\pm h/\pm k/\pm l$	31/7/22
θ range	θ_{min}–θ_{max}, deg	2.38 – 28.24
Absorption coefficient	μ, mm^{-1}	18.9
Data corrections		background, polarization, and Lorentz factors; numerical absorption correction by the program HABITUS [29]
Collected/unique reflections		11 408/1936
R_{int}/R_σ		0.092/0.054
Scattering factors		International Tables, Vol. C [32]
R_1 for 1508 reflections with $\lvert F_o\rvert > 4\,\sigma(F_o)$		0.041
R_1/wR_2 for all reflections		0.060/0.096
Goodness of Fit	GooF	1.049
Extinction	g	0.00007(4)
Residual electron density, ρ/e$^-\times10^{-6}$ pm^{-3} max./min.		1.72/−1.80

Table 2. Fractional atomic coordinates and equivalent isotropic displacement parameters U_{eq}[a] for $Na_2Y_3Cl_3[TeO_3]_4$.

Atom	Wyckoff site	x/a	y/b	z/c	U_{eq} (pm^2)
Na	8f	0.1660(3)	0.2741(7)	0.5749(4)	364(11)
Y1	4e	0	0.24830(16)	1/4	97(2)
Y2	8f	0.00077(5)	0.25128(12)	0.58531(6)	98(2)
Cl1	4d	1/4	1/4	1/2	296(8)
Cl2	8f	0.25029(15)	0.2537(4)	0.16897(19)	257(5)
Te1	8f	0.13595(3)	0.80045(9)	0.40416(4)	133(2)
Te2	8f	0.13302(3)	0.29522(9)	0.19722(4)	139(2)
O1	8f	0.0735(4)	0.5518(9)	0.3847(5)	138(12)
O2	8f	0.0867(4)	0.0156(9)	0.4265(5)	152(12)
O3	8f	0.0717(4)	0.0749(9)	0.7574(5)	149(12)
O4	8f	0.0700(4)	0.0524(9)	0.0914(5)	187(14)
O5	8f	0.0672(4)	0.4193(9)	0.2120(5)	168(13)
O6	8f	0.0851(4)	0.4842(9)	0.5774(5)	162(13)

[a] $U_{eq} = \frac{1}{3}[U_{22} + \frac{1}{\sin^2\beta}(U_{11} + U_{33} + 2U_{13}\cos\beta)]$.

Table 3. Motifs of mutual adjunction [33 – 35] for the crystal structure of $Na_2Y_3Cl_3[TeO_3]_4$[a].

	Na	Y1	Y2	Te1	Te2	CN
Cl1	2/1	0/0	0/0	0/0	0/0	2
Cl2	3/3	0/0	0/0	0/0	0/0	3
O1	1/1	1/2	1/1	1/1	0/0	4
O2	1/1	1/2	1/1	1/1	0/0	4
O3	0/0	1/2	1/1	1/1	0/0	3
O4	0/0	0/0	2/2	0/0	1/1	3
O5	0/0	1/2	1/1	0/0	1/1	3
O6	1/1	0/0	2/2	0/0	1/1	4
CN	7	8	8	3	3	

[a] CN = coordination number.

pated vibrational modes for the isolated ψ^1-tetrahedral $[TeO_3]^{2-}$ anions.

Diffuse reflectance spectroscopy

The diffuse reflectance spectroscopy measurements (DRS) were executed with a UV/Vis spectrometer (J&M, Essingen, Germany), which is equipped with an attachment including fiber optics. First, the data for a 0% reflectance were measured with the radiation source off. Second, the data for a 100% reflectance were recorded with $Ba[SO_4]$ as a white-reflectance standard. Afterwards, the sample reflectance was adjusted in the wavenumber range λ = 225 – 2500 nm (≡ 5.5 – 0.5 eV). The conversion of the measured data with the Kubelka–Munk function [36] gave the absorption data. The inflexion points of the function revealed the value for the optical band gap.

Fluorescence spectroscopy

The photoluminescence spectra of the europium-doped compound $Na_2Y_3Cl_3[TeO_3]_4$:Eu^{3+} were recorded on a Cary Eclipse fluorescence spectrophotometer (Varian, Darmstadt, Germany). The device is equipped with a pulsed xenon arc lamp (pulse length: 2 ms), and a photomultiplier with ex-

Na	–O6	227.4(8)	[1.28]	**Te2**	–O4	186.5(6)	[1.05]
	–O2	228.4(7)	[1.25]		–O5	187.7(6)	[1.01]
	–O1	274.2(7)	[0.26]		–O6	189.7(6)	[0.94]
	–Cl2	298.7(5)	[0.40]	**Te2**	–(O4,O5,O6)	103.7(4)	
	–Cl1	300.5(5)	[0.40]	**Cl1**	–Na	300.5(5) (2×)	[1.27]
	–Cl2′	321.4(5)	[0.14]	**Cl2**	–Na	298.7(5)	[1.40]
	–Cl2″	325.9(5)	[0.11]		–Na′	321.4(5)	[0.97]
Y1	–O5	229.2(6) (2×)	[1.18]		–Na″	325.9(5)	[0.89]
	–O1	233.3(6) (2×)	[1.07]	**Cl2**–(Na,Na′,Na″)		93.2(4)	
	–O3	241.5(6) (2×)	[0.87]	Na–**Cl1**–Na		180.0(3)	
	–O2	247.1(6) (2×)	[0.73]	Na–**Cl2**–Na′		101.6(2)	
Y2	–O3	229.6(6)	[1.22]	Na′–**Cl2**–Na″		107.9(2)	
	–O4	230.6(6)	[1.19]	Na–**Cl2**–Na″		124.5(2)	
	–O5	237.1(6)	[1.03]	O2–**Te1**–O3		88.2(3)	
	–O1	240.5(6)	[0.94]	O1–**Te1**–O3		88.2(3)	
	–O4′	240.7(6)	[0.93]	O1–**Te1**–O2		102.2(3)	
	–O6	243.8(6)	[0.85]	O5–**Te2**–O6		87.4(3)	
	–O2	244.5(6)	[0.85]	O4–**Te2**–O6		88.3(3)	
	–O6′	246.5(6)	[0.79]	O4–**Te2**–O5		100.9(3)	
Te1	–O1	188.0(6)	[1.02]				
	–O2	188.0(6)	[1.00]				
	–O3	189.2(6)	[0.98]				
Te1	–(O1,O2,O3)	102.5(4)					

Table 4. Selected internuclear distances (pm) with related ECoN values [33 – 35] in square brackets and angles (deg) for $Na_2Y_3Cl_3[TeO_3]_4$[a].

[a] ECoN = effective coordination number.

tended red-sensitivity ($\lambda = 300 - 850$ nm). The photoluminescence spectra were measured at room temperature and showed the typical $f \rightarrow f$ transitions for oxidic Eu^{3+}-doped compounds.

Results and Discussion

Crystal structure

$Na_2Y_3Cl_3[TeO_3]_4$ crystallizes monoclinically in space group $C2/c$ (no. 15) with the lattice parameters $a = 2380.69(14)$, $b = 552.76(3)$, $c = 1662.48(9)$ pm, $\beta = 134.045(3)^\circ$ and four formula units in each unit cell. Its crystal structure exhibits two crystallographically different Y^{3+} cations. Both are eightfold coordinated solely by O^{2-} anions in the shape of slightly distorted square antiprisms $[YO_8]^{13-}$ (Fig. 1, top). $(Y1)^{3+}$ occupies the Wyckoff position 4*e* and features yttrium-oxygen distances $d((Y1)^{3+}–O^{2-})$ from 229 to 247 pm. The polyhedron about the $(Y2)^{3+}$ cation at the Wyckoff site 8*f* is more distorted with yttrium-oxygen distances $d((Y2)^{3+}–O^{2-})$ ranging from 230 to 246 pm (for details see Table 4). These yttrium-oxygen distances are fairly long, but comparable to the reference data for the binary sesquioxide Y_2O_3 (bixbyite or *C* type [37]) with $d(Y^{3+}–O^{2-}) = 225 - 229$ pm and Y^{3+} in sixfold oxygen coordination. The $[YO_8]^{13-}$ polyhedra are interconnected *via* common edges to form chess board-like $^2_\infty\{[YO_{8/2}]^{5-}\}$ layers spreading out parallel to the (100) plane. According to the higher symmetry and the lower multiplicity of the 4*e* site, the polyhedron around $(Y1)^{3+}$ is connected in these layer to four surrounding polyhedra centered by $(Y2)^{3+}$. The crystal structure contains a single crystallographically unique Na^+ cation, which is situated on the 8*f* site and coordinated by three O^{2-} and four Cl^- anions (Fig. 2, bottom). The sodium-oxygen distances $d(Na^+–O^{2-})$ amount to 227 – 274 pm and the sodium-chlorine separations $d(Na^+–Cl^-)$ cover the range from 299 to 326 pm. The reference data for the binary compounds Na_2O [38] and NaCl [39] indicate sodium-oxygen distances $d(Na^+–O^{2-})$ of 240 pm (4×) for the *anti*-fluorite- and sodium-chlorine separations $d(Na^+–Cl^-)$ of 282 pm (6×) for the halite-type structure. The ternary oxide chloride Na_3OCl [40] in its *anti*-perovskite-type arrangement presents sodium-oxygen and sodium-chlorine distances of $d(Na^+–O^{2-}) = 225$ pm (2×) and $d(Na^+–Cl^-) = 318$ pm (4×), respectively. In comparison to these literature data, the calculated distance ranges for $Na_2Y_3Cl_3[TeO_3]_4$ are only a little longer. Parallel to the (100) plane, and thus to the $^2_\infty\{[YO_{8/2}]^{5-}\}$ layers (Fig. 3), the $[NaO_3Cl_4]^{9-}$ polyhedra are condensed *via* all $(Cl2)^-$ edges to build up $^1_\infty\{[Na_2O_6Cl_4]^{14-}\}$ strands, which subsequently become fused using all remaining $(Cl1)^-$ vertices to form $^2_\infty\{[Na_2O_6Cl_3]^{13-}\}$ layers (Fig. 4).

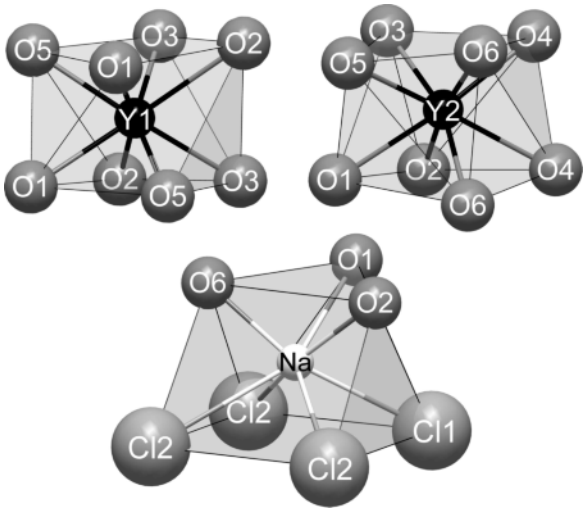

Fig. 2. The two crystallographically different Y^{3+} cations (top) and the unique Na^+ cation (bottom) in the crystal structure of $Na_2Y_3Cl_3[TeO_3]_4$ with their anionic coordination spheres.

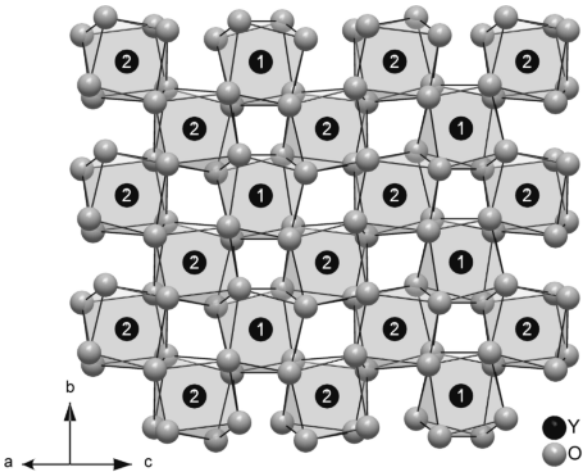

Fig. 3. $[YO_8]^{13-}$ polyhedra interconnected *via* four edges each to form $^2_\infty\{[YO_{8/2}]^{5-}\}$ layers parallel to the (100) plane in the crystal structure of $Na_2Y_3Cl_3[TeO_3]_4$.

The crystal structure includes two crystallographically different Cl^- anions. $(Cl1)^-$ at the 4d site is linearly coordinated by two Na^+ cations with $d((Cl1)^-–Na^+) = 301$ pm (2×) and $(Na^+–(Cl1)^–Na^+) = 180°$. The 8*f* site is occupied by $(Cl2)^-$ carrying three Na^+ cations, which establish a triangular plane with chlorine-sodium distances in a range from 299 to 326 pm. The distance from $(Cl2)^-$ to

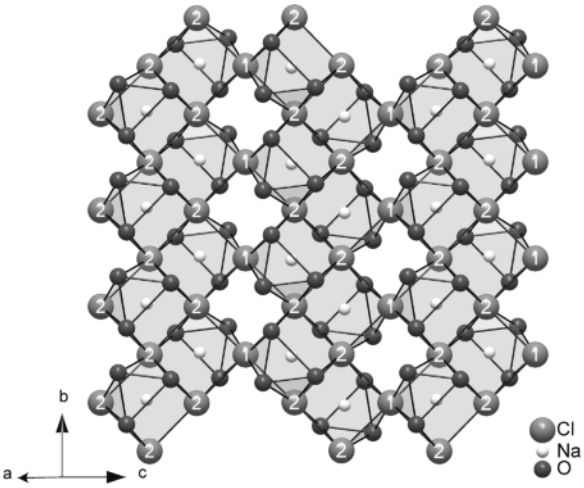

Fig. 4. $^2_\infty\{[Na_2O_6Cl_3]^{13-}\}$ layers parallel to the (100) plane formed by edge- and vertex-sharing of $[NaO_3Cl_4]^{9-}$ polyhedra in the crystal structure of $Na_2Y_3Cl_3[TeO_3]_4$.

the barycenter of the triangular $(Na^+)_3$ plane is about 93 pm (Fig. 5, bottom). Both Cl^- positions in the crystal structure of $Na_2Y_3Cl_3[TeO_3]_4$ are congruent to the sites of the Y^{3+} cations. Thus, they merely have to be shifted by $^1/_4$, 0, 0 perpendicular to the $^2_\infty\{[YO_{8/2}]^{5-}\}$ layers (Fig. 6). The two crystallographically different Te^{4+} cations (Fig. 5, top) are both located on 8*f* sites and connected to three O^{2-} anions each, forming complex anionic ψ^1-tetrahedral $[TeO_3]^{2-}$ units with non-bonding electron pairs (lone

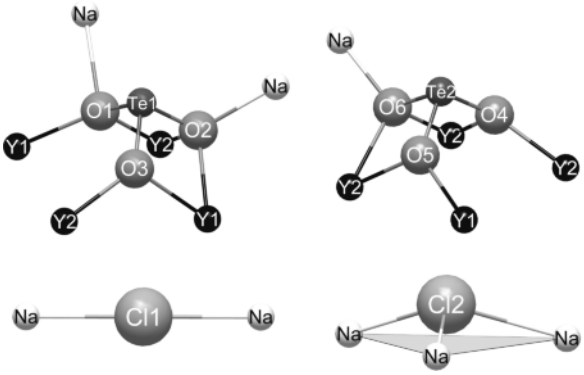

Fig. 5. The two crystallographically independent Te^{4+} cations forming ψ^1-tetrahedral $[TeO_3]^{2-}$ units (top) in the crystal structure of $Na_2Y_3Cl_3[TeO_3]_4$, and the two crystallographically independent Cl^- anions (bottom) coordinated by two or three Na^+ cations, respectively.

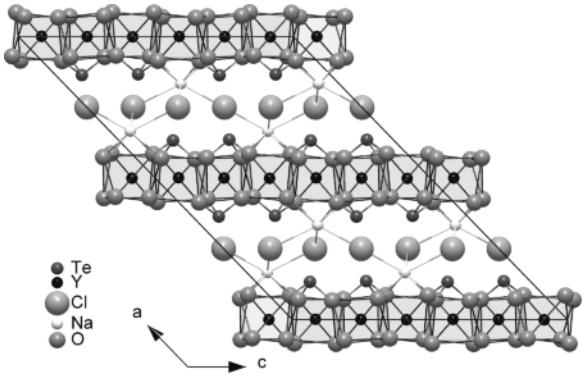

Fig. 6. Crystal structure of $Na_2Y_3Cl_3[TeO_3]_4$ as viewed along the [010] direction.

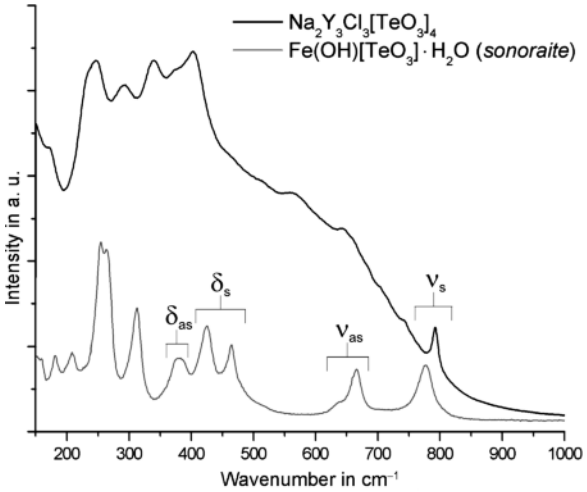

Fig. 7. Raman spectra of $Na_2Y_3Cl_3[TeO_3]_4$ (top) and the mineral sonoraite ($Fe(OH)[TeO_3] \cdot H_2O$): The four anticipated split-up modes for a distorted C_{3v} symmetry of the isolated $[TeO_3]^{2-}$ anions are visible in both spectra.

pairs). These pyramidal $[TeO_3]^{2-}$ anions reside above and below the $^2_\infty\{[YO_{8/2}]^{5-}\}$ layers. Thereby, the lone pairs point into the free space remaining between the $^2_\infty\{[YO_{8/2}]^{5-}\}$ layers (Fig. 6). Remarkably enough, the $[TeO_3]^{2-}$ groups remain *isolated* in the crystal structure, meaning that no secondary interactions among the $[TeO_3]^{2-}$ pyramids occur, as they have been reported for most structures of lanthanide(III) oxotellurates(IV) and their derivatives. The tellurium-oxygen distances $d(Te^{4+}–O^{2-})$ range from 187 to 190 pm (Table 4) and both Te^{4+} cations are 102 – 104 pm apart from their triangular $(O^{2-})_3$ planes. The binary tellurium oxides α-TeO_2 [41] and β-TeO_2 [42] ($d(Te^{4+}–O^{2-})$ = 190 – 208 pm) and TeO_3 ($d(Te^{6+}–O^{2-})$ = 185 pm) [43] display comparable distance ranges, although they consist of condensed networks of tellurium and oxygen with more highly coordinated tellurium cations in contrast to the isolated $[TeO_3]^{2-}$ anions in the crystal structure of $Na_2Y_3Cl_3[TeO_3]_4$. Finally, the three-dimensional network of the latter is built up from the layered assembly of the alternating $^2_\infty\{[YO_{8/2}]^{5-}\}$ and $^2_\infty\{[Na_2O_6Cl_3]^{13-}\}$ sheets by sharing common O^{2-} anions (Fig. 6). Thus the crystal structure of $Na_2Y_3Cl_3[TeO_3]_4$ is very similar, but not isotypic with the one of $Na_2Lu_3I_3[TeO_3]_4$ [24], where the Na^+ cations surprisingly have a higher coordination number of eight (four oxygen and iodine atoms each) instead of seven.

Raman spectroscopy

According to the C_{3v} symmetry of undistorted ψ^1-tetrahedral $[TeO_3]^{2-}$ anions, there are four vibrational modes ($2 \times A1$, $2 \times E$) to be expected in the Raman spectrum, analogous to the spectra of $[SeO_3]^{2-}$-containing compounds [44]. Due to the distortion of the $[TeO_3]^{2-}$ groups in the monoclinic crystal structure of $Na_2Y_3Cl_3[TeO_3]_4$, these modes can also split up. The Raman spectrum of $Na_2Y_3Cl_3[TeO_3]_4$ is depicted in Fig. 7 in comparison to that of the mineral sonoraite ($Fe(OH)[TeO_3] \cdot H_2O$) [45], which also contains isolated pyramidal $[TeO_3]^{2-}$ units. In both spectra the anticipated and split-up vibrational modes of the $[TeO_3]^{2-}$ anions can be observed [46], but they are superimposed partially by metal-oxygen vibrational modes (not indicated in the spectra), and by a fairly high background noise. In the spectrum of the title compound the $A1$ symmetric stretching mode ν_s emerges at 793 cm^{-1} (medium). The asymmetric stretching modes ν_{as} (E) follow at 643 (weak) and 657 cm^{-1} (shoulder, very weak), both strongly superimposed by the background. The symmetric bending mode δ_s ($A1$) appears at 403 cm^{-1} (medium) with a shoulder at 460 cm^{-1} (very weak). The asymmetric bending modes δ_{as} (E) are visible at 340 cm^{-1} (medium) with a shoulder at 333 cm^{-1} (very weak).

Diffuse reflectance spectroscopy

The DRS measurements [47, 48] were performed to determine the optical band gap for the undoped phase

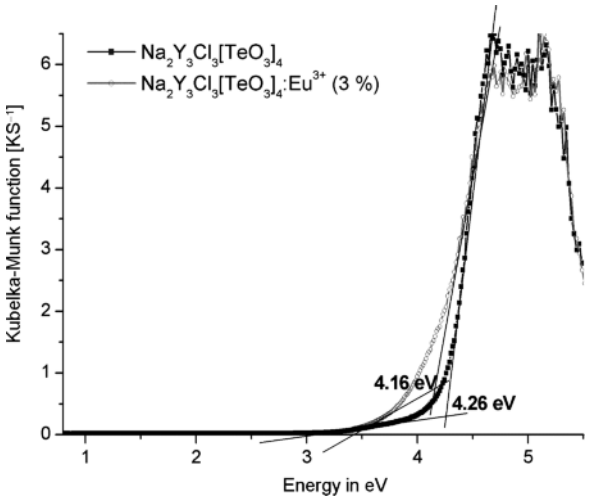

Fig. 8. Diffuse reflectance spectra of undoped (black curve) and Eu^{3+}-doped (gray curve) $Na_2Y_3Cl_3[TeO_3]_4$ samples converted to the Kubelka-Munk functions to yield the optical band gaps.

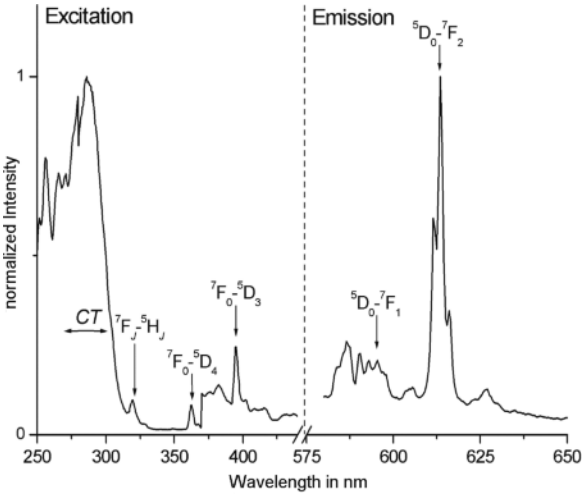

Fig. 9. Fluorescence spectra of $Na_2Y_3Cl_3[TeO_3]_4$:Eu^{3+} emphasizing the excitation spectrum (left) and the emission spectrum (right).

$Na_2Y_3Cl_3[TeO_3]_4$ and the europium-doped compound ($Na_2Y_3Cl_3[TeO_3]_4$:Eu^{3+}). Therefore, the absorption was converted to the Kubelka-Munk function [36] (Fig. 8), which shows at the intersection of the inflexion points of the function an optical band gap of $E_g = 4.26$ eV for the undoped and $E_g = 4.16$ eV for the Eu^{3+}-doped sample, in perfect agreement with the missing color of both samples. These findings correspond with wavelengths of $\lambda = 291$ ($\equiv 4.26$ eV) and 298 nm ($\equiv 4.16$ eV), respectively, and can also clearly be seen in the fluorescence excitation spectrum (Fig. 9) of the undoped sample as a broad charge-transfer band (indicated as CT). Moreover, the DRS measurements have shown that Eu^{3+}-doping has only little effects on the crystal structure and the band gap ($\Delta E_g = 0.10$ eV). Therefore, the charge-transfer region depends not exclusively on the electronic $f \rightarrow f$ and $O^{2-} \rightarrow Eu^{3+}$ CT transitions, but also results from the electronic $s \rightarrow p$ transitions at the Te^{4+} cation with its lone-pair, addressable as an *inorganic antenna effect*.

Fluorescence spectroscopy

Under UV lamp irradiation with an excitation wavelength of $\lambda = 254$ nm, $Na_2Y_3Cl_3[TeO_3]_4$:Eu^{3+} shows a bright red luminescence. The emission lines of Eu^{3+} in the red spectral region result from the excited $^5D_0$ state to the ^7F_J ground states [49] with $J = 0-6$ and also higher excited states ($^5D_1$, $^5D_2$, $^5D_3$) of the electronic $4f^6$ configuration of the Eu^{3+} cation. For comparison, the intensities of both the excitation and the emission spectrum were normalized. The excitation spectrum presents a broad band between 250 and 315 nm, including the host-structure excitation (between 250 and 260 nm) [50] as well as electronic $d \rightarrow f$ transitions of the Eu^{3+} cation and $O^{2-} \rightarrow Eu^{3+}$ ligand-to-metal charge-transfer (LMCT) (from 260 to 315 nm, indicated as CT in Fig. 9). According to the DRS measurements (Fig. 8), the Te^{4+} cations additionally contribute to the charge-transfer band with $s \rightarrow p$ transitions of their lone pairs as inorganic antennae, comparable to the complex anionic $[MoO_4]^{2-}$ units in $YF[MoO_4]$ and $YCl[MoO_4]$ [51]. The excitation at 320 nm results from $^7F_J \rightarrow {}^5H_J$ transitions of higher excited states, followed by the $^7F_0 \rightarrow {}^5D_4$ transition at 362 nm and the $^7F_0 \rightarrow {}^5D_3$ transition at 395 nm [49, 50, 52]. The emission spectrum features the $^5D_0 \rightarrow {}^7F_0$ transition at 586 nm with only weak intensity due to the forbidden electric dipole transition and to the allowed magnetic dipole transition, both being always much less intense. Between 590 and 598 nm the allowed electric dipole transitions $^5D_0 \rightarrow {}^7F_1$ are also observed with a low intensity, depending mainly on the chemical environment. The most intense transition is represented by the $^5D_0 \rightarrow {}^7F_2$ emission line at 613 nm, followed at about 627 nm by the forbid-

den $^5D_0 \rightarrow {}^7F_3$ electric dipole transition, again magnetically allowed and therefore very weak [49, 50]. Due to the fact that the $^5D_0$ state can not be split by the crystal field ($J = 0$), the split emission lines need to originate from the crystal-field splitting of the ^7F_J states. The most prominent $^5D_0 \rightarrow {}^7F_2$ emission emerges as a triplet in the spectrum. Hence, it is not possible to determine whether the Eu^{3+} cations prefer to occupy the site of $(Y1)^{3+}$ or $(Y2)^{3+}$.

Conclusion

The crystal structure of $Na_2Y_3Cl_3[TeO_3]_4$ was determined by single-crystal and powder X-ray diffraction measurements. Its powder pattern also proved the new quintenary oxotellurate(IV) to be obtainable phase-pure. The crystal structure includes isolated ψ^1-tetrahedral $[TeO_3]^{2-}$ anions, which could also be detected by Raman spectroscopy. The europium-doped compound $Na_2Y_3Cl_3[TeO_3]_4$:Eu^{3+} was also synthesized. According to its fluorescence performance, it is a promising red phosphor exhibiting the prominent transitions of an Eu^{3+}-doped compound and a broad charge-transfer owing to an *inorganic antenna effect* of the $[TeO_3]^{2-}$ anions. Diffuse reflectance spectroscopy did verify that Eu^{3+}-doping has only minor effects on the crystal structure of the colorless compound, so that the optical band gaps of the undoped and doped samples are very similar and prove the significance of an inorganic antenna effect.

Acknowledgement

The authors like to thank the State of Baden-Württemberg (Stuttgart, Germany) and the Fonds der Chemischen Industrie (Frankfurt am Main, Germany) for financial support. Moreover, we are grateful to Dr. Sabine Strobel for the collection of the X-ray diffraction intensity data set for the single crystal.

[1] M. J. Redman, W. P. Binnie, J. R. Carter, *J. Less-Common Met.* **1968**, *16*, 407.
[2] S. F. Meier, Doctoral Thesis, University of Stuttgart, Stuttgart **2002**.
[3] S. F. Meier, Th. Schleid, *Z. Kristallogr.* **2002**, *Suppl. 19*, 113.
[4] P. Höss, Doctoral Thesis, University of Stuttgart, Stuttgart **2009**.
[5] S. F. Meier, P. Höss, Th. Schleid, *Z. Anorg. Allg. Chem.* **2009**, *635*, 768.
[6] P. Höss, S. F. Meier, Th. Schleid, *Z. Anorg. Allg. Chem.* **2013**, *639*, 2548.
[7] A. Castro, R. Enjalbert, D. Lloyd, I. Rasines, J. Galy, *J. Solid State Chem.* **1990**, *85*, 100.
[8] F. A. Weber, S. F. Meier, Th. Schleid, *Z. Anorg. Allg. Chem.* **2001**, *627*, 2225.
[9] I. Ijjaali, C. Flaschenriem, J. A. Ibers, *J. Alloys Compd.* **2003**, *354*, 115.
[10] S. F. Meier, Th. Schleid, *Z. Naturforsch.* **2004**, *59b*, 881.
[11] P. Höss, S. F. Meier, Th. Schleid, *Z. Kristallogr.* **2004**, *Suppl. 21*, 162.
[12] Y.-L. Shen, J.-G. Mao, *J. Alloys Compd.* **2004**, *385*, 86.
[13] P. Höss, G. Starkulla, Th. Schleid, *Acta Crystallogr.* **2005**, *E 61*, i 113.
[14] F. A. Weber, Th. Schleid, *Z. Kristallogr.* **2000**, *Suppl. 17*, 136.
[15] F. A. Weber, S. F. Meier, Th. Schleid, *Z. Anorg. Allg. Chem.* **2001**, *627*, 2225.
[16] S. F. Meier, Th. Schleid, *Z. Naturforsch.* **2005**, *60b*, 720.
[17] P. Höss, S. F. Meier, Th. Schleid, *Z. Kristallogr.* **2005**, *Suppl. 22*, 153.
[18] P. Höss, Th. Schleid, *Z. Anorg. Allg. Chem.* **2007**, *633*, 1391.
[19] P. Höss, Th. Schleid, *Z. Kristallogr.* **2006**, *Suppl. 24*, 173.
[20] S. F. Meier, Th. Schleid, *Z. Anorg. Allg. Chem.* **2006**, *632*, 1759.
[21] P. Höss, M. Jegelka, Th. Schleid, *Z. Anorg. Allg. Chem.* **2006**, *632*, 2148.
[22] S. F. Meier, Th. Schleid, *Z. Anorg. Allg. Chem.* **2003**, *629*, 1575.
[23] S. F. Meier, Th. Schleid, *Z. Anorg. Allg. Chem.* **2002**, *628*, 526.
[24] S. Zitzer, Th. Schleid, *Z. Anorg. Allg. Chem.* **2010**, *636*, 1050.
[25] S. Zitzer, Doctoral Thesis, University of Stuttgart, Stuttgart **2012**.
[26] J. Dhanaraj, R. Jagannathan, D. C. Trivedi, *J. Mater. Chem.* **2003**, *13*, 1778.
[27] A. K. Levine, F. C. Palilla, *Appl. Phys. Lett.* **1964**, *5*, 118.
[28] P. Höss, A. Osvet, F. Meister, M. Batentschuk, A. Winnacker, Th. Schleid, *J. Solid State Chem.* **2008**, *181*, 2783.

[29] W. Herrendorf, H. Bärnighausen, ProgramHABITUS, Universities of Karlsruhe and Gießen, Karlsruhe **1993**, Gießen **1996**.
[30] G. M. Sheldrick, SHELXS/L-97, Programs for Crystal Structure Determination, University of Göttingen, Göttingen (Germany) **1997**.
[31] G. M. Sheldrick, *Acta Crystallogr.* **2008**, *A64*, 112.
[32] E. Prince (Ed.), *International Tables for Crystallography*, Vol. C: Mathematical, Physical and Chemical Tables, Kluwer Academic Publishers, Dordrecht **2004**.
[33] R. Hoppe, *Angew. Chem., Int. Ed. Engl.* **1966**, *5*, 95.
[34] R. Hoppe, *Angew. Chem., Int. Ed. Engl.* **1970**, *9*, 25.
[35] R. Hoppe, *Angew. Chem., Int. Ed. Engl.* **1980**, *19*, 110.
[36] P. Kubelka, F. Munk, *Z. Techn. Phys.* **1931**, *12*, 593.
[37] E. Zintl, A. Harder, B. Dauth, *Z. Anorg. Allg. Chem.* **1931**, *191*, 88.
[38] I. G. Brauer, H. Gradinger, *Z. Anorg. Allg. Chem.* **1954**, *276*, 209.
[39] W. H. Bragg, W. L. Bragg, *Z. Anorg. Allg. Chem.* **1915**, *90*, 167.
[40] K. Hippler, S. Sitta, P. Vogt, H. Sabrowsky, *Acta Crystallogr.* **1990**, *C46*, 736.
[41] O. Lindquist, *Acta Chem. Scand.* **1968**, *22*, 977.
[42] H. Beyer, *Z. Kristallogr.* **1967**, *124*, 228.
[43] M. A. K. Ahmed, H. Fjellvag, A. Kjekshus, *J. Chem. Soc., Dalton Trans.* **2000**, *2000*, 4542.
[44] M. S. Wickleder in *Handbook on the Physics and Chemistry of Rare Earths*, Vol. 35, (Eds.: J.-C. G. Bünzli, K. A. Gschneidner, Jr., V. K. Pecharsky), Elsevier Science Publishers, Amsterdam **2005**.
[45] R. T. Downs, *The* RRUFF*Project: An Integrated Study of the Chemistry, Crystallography, Raman and Infrared Spectroscopy of Minerals*, Department of Geoscience, University of Arizona, Tucson (AZ) **2006**.
[46] R. L. Frost, E. C. Keeffe, *J. Raman Spectrosc.* **2009**, *40*, 133.
[47] G. Kortüm, *Reflectance Spectroscopy*, Springer-Verlag, Berlin, New York **1969**.
[48] G. Kortüm, W. Braun, G. Herzog, *Angew. Chem., Int. Ed. Engl.* **1963**, *2*, 333.
[49] S. Cotton, *Lanthanide and Actinide Chemistry*, John Wiley & Sons Ltd., Hoboken (NJ) **2006**.
[50] G. Blasse, B. C. Grabmaier, *Luminescent Materials*, Springer-Verlag, Berlin, New York **1994**.
[51] I. Hartenbach, Th. Schleid, S. Strobel, P. K. Dorhout, P. Nockemann, K. Binnemans, *Inorg. Chem.* **2008**, *47*, 3728.
[52] D. Uhlich, Doctoral Thesis, University of Osnabrück, Osnabrück **2009**.